Sensors and Actuators B 222 (2016) 339–346

Contents lists available at ScienceDirect

Sensors and Actuators B: Chemical

journal homepage: www.elsevier.com/locate/snb

Hygroscopic polymer microcavity fiber Fizeau interferometer incorporating a fiber Bragg grating for simultaneously sensing humidity and temperature

Cheng-Ling Lee*, Yan-Wun You, Jia-Heng Dai, Jui-Ming Hsu, Jing-Shyang Horng

Department of Electro-Optical Engineering, National United University, Miaoli 360, Taiwan, ROC

ARTICLE INFO

Article history:
Received 2 June 2015
Received in revised form 12 August 2015
Accepted 18 August 2015
Available online 21 August 2015

Keywords:
Fiber optic sensor
Relative humidity
Polymer
Fiber Fizeau interferometer
Hygroscopic

ABSTRACT

This work proposes a hygroscopic polymer microcavity fiber Fizeau interferometer (PMFFI) incorporating a fiber Bragg grating (FBG) for the simultaneous measurement of relative humidity (*RH*) and temperature (*T*). The PMFFI was fabricated by attaching the hygroscopic polymer to a single-mode fiber endface to form a low-finesse Fabry–Perot resonant microcavity. This work is the first to investigate polymer of the Norland Optical Adhesive (NOA) series with particular porous structures that responds well to the moisture and can thus be used in the fiber-optic sensing of relative humidity. Additionally, the NOA materials have a high thermal expansion coefficient and so can be used in the highly sensitive measurement of temperature. The adsorption/desorption of water molecules and variations in temperature both change the optical path of the microcavity, shifting the fringes in the interference spectra. Incorporating a general FBG that is nonreactive to *RH* but sensitive to *T* judges the variation in *T*. The combined sensor supports the simultaneous measurement of both parameters *RH* and *T* by gauging of the individual spectral responses of PMFFI and FBG, respectively. Experimental results demonstrate that the *RH* and *T* can be simultaneously measured with high sensitivity and accuracy using the proposed sensing configuration.

1. Introduction

Relative humidity (*RH*) is the amount of water vapor in air relative to the amount of water vapor in saturation at a static temperature (*T*). *RH* depends mainly on the *T* of the environment. The simultaneous measurement of both *RH* and *T* has important applications, such as in semiconductors, food processing, and biomedical and industrial technologies. These two physical properties of the environment can affect the quality and yield of manufactured products. Therefore, the simultaneous measurement of these two parameters is becoming increasingly important. Although the *RH*/*T* measurement instruments that are based on the electronic devices are the commonly used, however, they will soon be replaced by sensors that are based on photonic structures. The reason is that the electronic humidity sensors do not perform well in harsh environments, such as in the presence of corrosive substances or high temperature. The fiber optic sensors have always been regarded as sensitive and potential candidates owing to their many advantages, including non-electrical operation, tiny size, high sensitivity, corrosion resistance, effectiveness in remote measurement and rapid response [1–33]. However, few all-silica-based fiber optic humidity sensors have rarely been developed because their main constituent material, silica, is not a favorable hygroscopic substance. Hygroscopic materials, such as agarose [1,13,20,22,24,27], polyvinyl alcohol (PVA) [14,16,18,19,21,23,29,30], polymeric substances [2,3,5,6,9,15,26] or others [7,10,12,17,28] have been coated onto the main elements of the fiber sensors. Optical signals are modulated by the physical and chemical reactions of these materials to the *RH* of the environment. In relevant studies, special fibers, such as those with hollow cores (HCF) [12], multimode fibers (MMF) [9,17,23,29], photonic crystal fibers (PCF) [8,13,16,18,19,22,24,27] and plastic optical fibers (POF) [3], have been used for measuring humidity. Regardless of the hygroscopic materials that are used in the fibers, the sensing mechanism is usually based on very slight variations of the refractive indices (RI) and thicknesses of the hygroscopic materials upon the absorption of H_2O molecules [1–32]. Thus, the types of interferometric fiber sensors are especially suitable for the extremely insignificant changes of the RI and thicknesses of the hygroscopic materials due to their miniature size, high sensitivity and very high resolution. *RH* depends strongly on *T*. Thus, the variations in *RH* can be well evaluated only if *T* can be measured at the same time. Accordingly, the simultaneous

* Corresponding author.
E-mail address: cherry@nuu.edu.tw (C.-L. Lee).

http://dx.doi.org/10.1016/j.snb.2015.08.086
0925-4005/© 2015 Published by Elsevier B.V.

measurement of the *RH* and *T* parameters of a system is of scientific and technological importance. Some fiber humidity sensors that are incorporated into fiber gratings have been developed with hybrid structures for simultaneously sensing other physical parameters. These works have especially focused on the simultaneous sensing of *RH* and *T* parameters [2,11,19,24,30].

This work develops a very simple, easy, and flexible probetype polymer micro-cavity fiber Fizeau interferometer in which is incorporated a general FBG for the simultaneous measurement of *RH* and *T*. The simultaneous measurement is based on the different responses of the PMFFI and the FBG to the *RH* and *T*. The PMFFI is coated with a layer of Norland Optical Adhesive (NOA) polymer by a convenient and efficient UV-cured method, as presented in Fig. 1. In this work, for the first time, materials form the NOA series are utilized in the fibers with favorable hygroscopic properties [31,32] and strong responses to *T* [33]. The NOA that is used herein is an optical gel whose porosity causes physical adsorption and desorption of water molecules from and to the surroundings [34]. Therefore, the optical path of the Fizeau cavity varies owing to H_2O adsorption and desorption as the humidity changes. Hence, the proposed device can be expected to be a good humidity sensor. The NOA 61 also has a high sensitivity to *T* owing to its high thermal expansion coefficient (TEC) of $2.2 \times 10^{-4}\,^{\circ}C^{-1}$ [35] and has much higher RI than that of fiber, so it is more suitable for use in our device. Besides, it is designed to give an excellent bond to glass surfaces and may be polished after UV-curing [36]. Thus, the polymer surface can be treated as smooth mirror so the surface roughness is ignored. By incorporating a simple bare FBG that is almost unaffected by humidity and so exhibits a spectral shift only with a variation in *T*, allows the simultaneous measurement of both *RH* and *T* and the individual responses of the sensor to both parameters to be evaluated.

2. Sensing principle

The Fizeau interferometer is a Fabry–Perot interferometer (FPI) whose cavity has a low reflectivity. Thus, sensing principle using the proposed PMFFI exploits the characteristics of the low-finesse fiber FPI. The polymer coating of the NOA series on the SMF swells or shrinks in response to ambient *RH*/*T* changes, affecting the optical length of the Fabry–Perot cavity as well as the phase difference between the consecutively reflected light beams. Monitoring the variation of interference fringes that are reflected from the two interfaces yields obtain the information about the changes of *RH*/*T* from the ambient space. Most importantly, this work is the first in which hygroscopic characteristics of the porous structures of the NOA series of materials are exploited to sense changes in *RH* and *T* [31–33].

In the configuration of the sensor that is shown in Fig. 1, when the Fresnel reflectivity of the interfaces is low, the behavior of the cavity can be approximated using a two-beam interferometric model, given by the equation,

$$r = r_1 + r_2 \pm 2\sqrt{r_1 r_2}\cos(\phi) \quad (1)$$

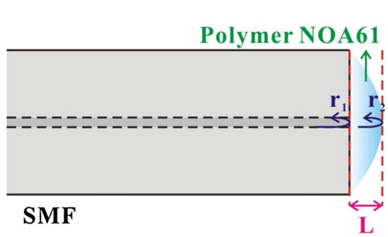

Fig. 1. Configuration and operating principle of PMFFI.

where r is the reflected intensity of the interference signal; r_1 and r_2 denotes the intensities that are reflected at the interfaces, and ϕ denotes the optical phase of the interferometer, given by Eq. (2).

$$\phi = \frac{4\pi n L}{\lambda} \quad (2)$$

where n is the refractive index of the medium NOA 61 that is formed as the Fizeau cavity and λ is wavelength of the light source. The phase difference between both interference beams depends upon the optical path nL, where L is the thickness and n refractive index of the cavity. The periodicity of the spectral fringes of the spectra can be expressed using the free spectral range (FSR),

$$\mathrm{FSR} = \frac{\lambda_m \lambda_{m+1}}{2nL} \quad (3)$$

$\mathrm{FSR} \cong \lambda_{m+1} - \lambda_m$, where m is an integer and λ_m and λ_{m+1} are the central wavelengths of the two peaks/dips adjacent to the mth dip in the spectrum. Changes in the cavity that are caused by *RH*/*T* variations cause phase shifts in the interference signal that can be retrieved by tracking the wavelength shift of the interference spectrum using an optical spectrum analyzer (OSA). Thus, the mth wavelength (λ_m) of the spectral minimum with the condition $\varphi = 2m\pi$ is given by the expression of Eq. (4).

When the PMFFI sensor is exposed to the different *RH*/*T* levels, the NOA 61 cavity expands/shrinks, changing the optical length (nL) of the cavity, shifting the λ_m, which satisfies,

$$\lambda_m = \frac{2nL}{m} \quad (4)$$

The incorporated FBG whose grating written in the core of SMF is insensitive to humidity but sensitive to *T*. Owing to the high sensitivity of the PMFFI to *T*, *T* and *RH* can be simultaneously measured using the combination of the PMFFI and the FBG. If the *T* and *RH* change, the wavelength shifts that are caused by both the FBG and the PMFFI can be respectively estimated by using the following equations.

$$\frac{\Delta\lambda_{FBG}}{\lambda_{FBG}} = \frac{1}{\Lambda}\frac{\partial \Lambda}{\partial T}\Delta T + B\Delta RH = A\Delta T + B\Delta RH \quad (5a)$$

$$\frac{\Delta\lambda_{PMFFI}}{\lambda_{PMFFI}} = \frac{1}{d}\frac{\partial d}{\partial T}\Delta T + D\Delta RH = C\Delta T + D\Delta RH \quad (5b)$$

where A, C and B, D are the temperature and humidity sensitivity coefficients of the PMFFI and the FBG, respectively; d and Λ denote the cavity of the PMFFI and grating period of the FBG, respectively. The coefficients A, B, C and D can be determined by measuring the responses of spectral sensitivities of the PMFFI and the FBG in the combined device to variations in *T* and *RH*, respectively. Then, the matrix inversion method is used to obtain the variations of temperature (ΔT) and relative humidity (ΔRH) simultaneously from the wavelength shifts of the PMFFI ($\Delta\lambda_{PMFFI}$) and the FBG ($\Delta\lambda_{FBG}$), respectively. The relationship between the above parameters is as follows.

$$\begin{pmatrix} \Delta T \\ \Delta RH \end{pmatrix} = \begin{pmatrix} A & B \\ C & D \end{pmatrix}^{-1} \begin{pmatrix} \dfrac{\Delta\lambda_{FBG}}{\lambda_{FBG}} \\ \dfrac{\Delta\lambda_{PMFFI}}{\lambda_{PMFFI}} \end{pmatrix} \quad (6)$$

Eq. (6) can be simplified as,

$$\begin{pmatrix} \Delta T \\ \Delta RH \end{pmatrix} = \begin{pmatrix} A' & B' \\ C' & D' \end{pmatrix}^{-1} \begin{pmatrix} \Delta\lambda_{FBG} \\ \Delta\lambda_{PMFFI} \end{pmatrix} \quad (7)$$

where A', C', B' and D' are the normalized coefficients of the sensitivities of the FBG to *T* and *RH* and of the PMFFI to *T* and *RH*, respectively. As a result, the obtained variations of the center wavelength of the FBG ($\Delta\lambda_{FBG}$) and the shifts of peaks/dips of the PMFFI

($\Delta\lambda_{PMFFI}$) can easily and simultaneously yield the changes of *RH* and *T*.

3. Experimental

3.1. Fabrication of PMFFI

The configuration of the sensor is based on the simple two-beam interferometric mechanism. The polymer NOA61 acts as a microcavity that generates low-finesse interference by reflecting from its first and second interfaces, as presented in Fig. 1. When the sensing probe is placed in the testing environment, the interference spectra were changed by the adsorption and desorption of H_2O molecules. To fabricate the PMFFI, a sensor probe was formed by manually depositing a layer of NOA 61 on the endface of an SMF28 fiber and the deposition process was monitored by using a CCD microscope. The NOA 61 is a clear, colorless, liquid photopolymer that is cured by exposure to ultraviolet (UV) light. The curing process transforms the liquid NOA61 into a full solid and a well-bonded polymer structure. The adhesive force between the SMF and the polymer is strong when the latter is fully cured. In the experiment herein, the NOA 61 on the endface of the SMF becomes fully solid upon exposure to UV light with an intensity of around 5 mW/cm^2 for 30 s at room temperature. However, in this situation, the NOA 61 does not reached its optimum adhesion to glass, even with complete curing. Therefore, the aging process was executed herein to form chemical bonds between the glass and the NOA 61 polymer [36]. Accordingly, the good adhesion, improved solvent resistance and an ability to withstand temperatures of up to 200 °C are achieved. These superior characteristics are very important in the fabrication of high-quality optical devices and the achievement of long-term performance in a changing environment. For most humidity fiber sensors that are listed in the references, the preparations of the hygroscopic materials are complicated and the coatings of these hygroscopic materials on the fibers are difficult. In contrast, the NOA interferometric sensors developed herein are fabricated using easily and rapidly technique by manually overlaying a NOA layer on the endface of a fiber with a convenient and efficient UV-curing method.

3.2. Measurement setup

Fig. 2 shows the proposed fiber-optic multiple-sensing system. The measurement system comprises an optical spectrum analyzer, OSA; a broadband light source, BLS; the proposed PMFFI and a general FBG sensing probe. A chamber with controlled temperature and humidity and a 2 × 2 optical fiber coupler are also used. The light that is emitted from the BLS is firstly coupled into a coupler and divided into two parts. One beam of light propagates to the fabricated PMFFI and the other is incident on the FBG probe. The PMFFI generates quasi-sinusoidal interference patterns over a very wide range of wavelengths. The light from the FBG probe with a specific central Bragg wavelength is reflected. These two reflected spectra are collected by the coupler and detected by the OSA. An Advantest Q8384 OSA is used to record the optical spectra. The OSA has a wide dynamic range of 60 dB and a high wavelength resolution of 0.01 nm. The used BLS of the type OLSWB-OESCLU-FA is from the Opto-Link Corporation Ltd. It comprises a series of superluminescent light emitting diodes whose power was synchronously monitored during the experiment to ensure stability. The great merit of the proposed interferometric sensing scheme of the fiber sensor is that it does not require alignment of the propagated optical light. The sensing system also does not need to be operated on an optical table since the sensor developed herein can be easily packaged in a commercial fiber U-groove and was stable even under vibrations or in flowing air conditions.

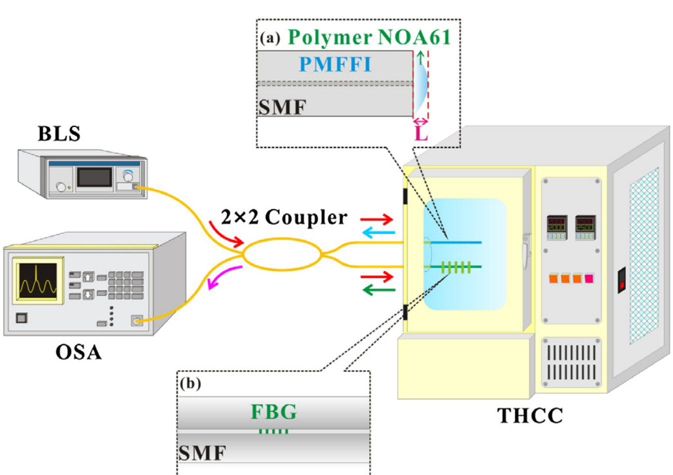

Fig. 2. Experimental setup for simultaneously measuring *RH* and *T*. Insets (a) and (b) schematically depict sensor heads of (a) PMFFI and (b) FBG, respectively.

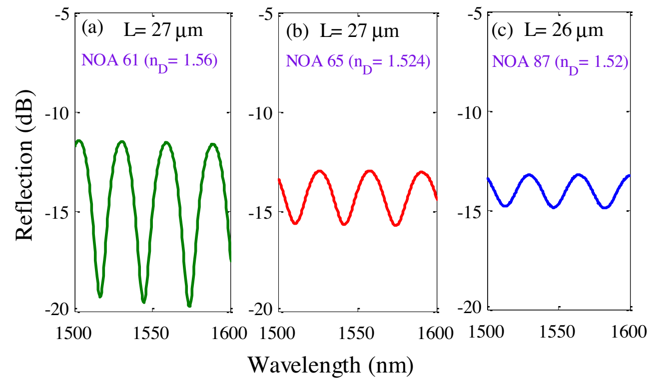

Fig. 3. Spectral responses of fabricated PMFFIs with different types of NOA materials of (a) NOA 61, (b) NOA 65, and (c) NOA 87.

3.3. Characteristics of the PMFFIs

The main advantage of the proposed PMFFI is that its structure can be easily modified by controlling the amount of the attached NOA. There are many types of NOA series with specific features [36]. NOA 61 (n_D = 1.56), NOA 65 (n_D = 1.524), and NOA 87 (n_D = 1.52) are typically used in the fields of optics and fiber communications. The RI of NOA 61 is much higher than those of the silica fiber and air and consequently the NOA-microcavity can produce higher Fresnel reflections; it is therefore more suitable for use in our device proposed herein. Fig. 3 presents the optical spectra of three NOA-based sensors with the same structure (cavity length). Sensor (a) with high fringe visibility was realized using the material of NOA 61. Hence, the material of NOA 61 was chosen to fabricate the proposed sensor. Fig. 4 shows different structures of the PMFFIs can be fabricated for particular applications. The Fig. 4(a) shows side-view of the microphotographs of the sensor endface with different microcavity of the polymers. The arc shape of the fabricated polymer surface is created by the cohesive force of the NOA61 liquid. The results of Fig. 4(a) demonstrate that the thin polymer film with a thickness from 10 μm to 42 μm can be effectively attached to the endface of the SMF. The corresponding interference patterns of the fabricated PMFFIs in Fig. 4(a) are measured and plotted in Fig. 4(b). Two Fresnel beams from the interfaces of the polymer micocavity can yield pure sinusoidal interference patterns. The spectral interference fringes reveal that a longer cavity has a denser interference

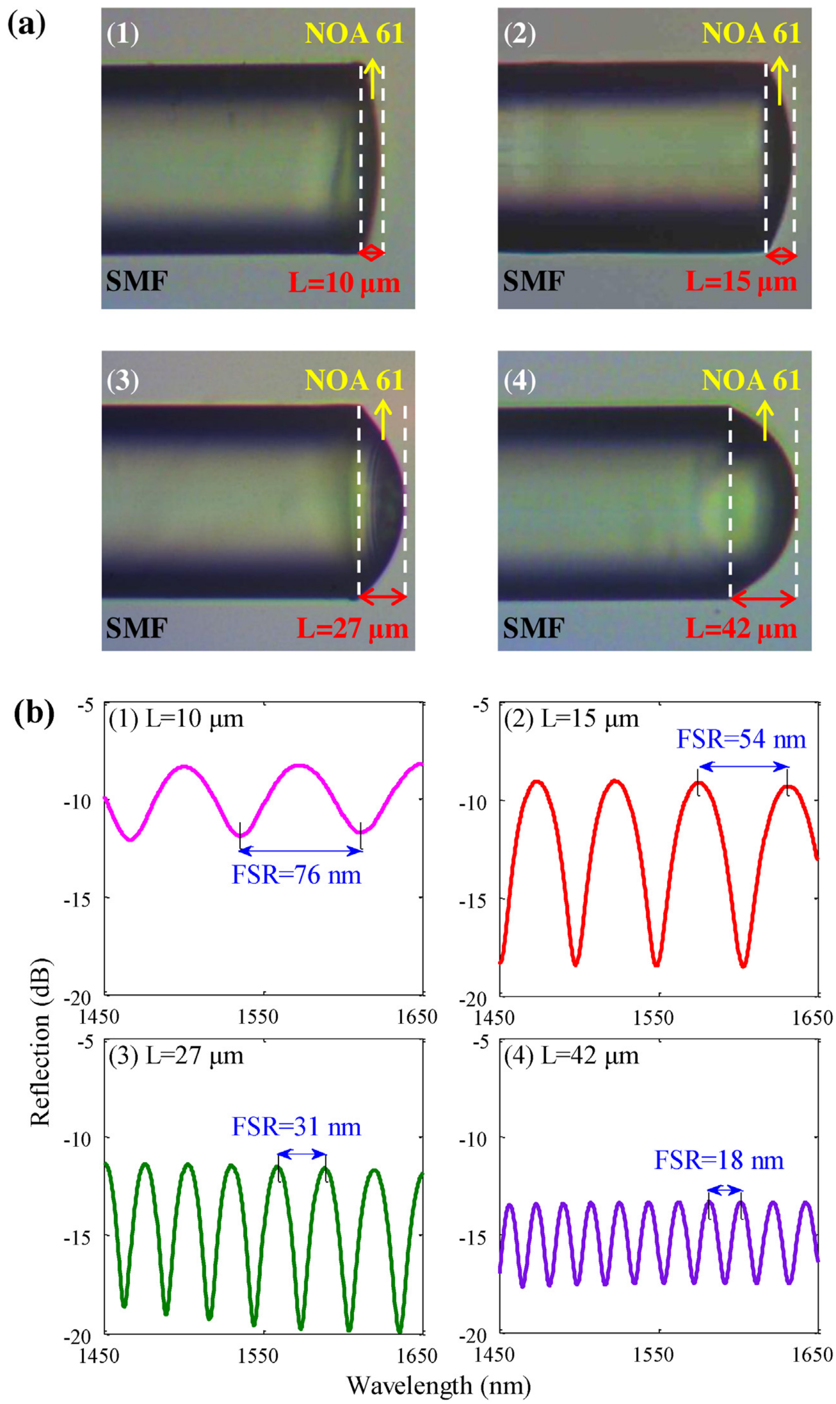

Fig. 4. (a) Microphotographs and (b) spectral responses of fabricated PMFFIs with cavity lengths, L of (1) 10 μm, (2) 15 μm, (3) 27 μm and (4) 42 μm.

pattern and a shorter free spectral range over a given range of wavelengths. The overall insertion loss is in the range 7–14 dB for PMFFIs with different values of d. The fringe visibilities also vary with the value of d of the device. Several factors influence the visibility of the fringes from the devices, such as the quality of fabrication (manually coating and UV-curing), the geometry of the NOA 61 polymer cavity and the RI of the NOA materials. The first factor does not need to be discussed owing to the uncertainties associated with human skills. The second factor is considered to be the most important to affect visibility when the NOA materials are specified. According to Eq. (1), the interference performance is optimal and the fringe visibility is maximal when the intensities of two interference beams are equal. The Fresnel reflection from the first interface, fiber/NOA, is weaker than that of the second interface, NOA/air. Theoretically, when an optical beam propagates from an SMF into a NOA-polymer zone, its mode field expands. The expanded beam was reflected from the second interface, NOA/air, and some of the light is received by the acceptance cone of the SMF, re-entering into the fiber core. Therefore, the amount of r_2 that re-coupled into the core is strongly related to the visibility of the fringes of the interference spectra. In the Fig. 4(a) and (b), sensor (1) has a very thin cavity and poor fringe visibility because most of the r_2 is re-coupled to the core. The long cavity with the long propagating optical path in sensor (4) yields weaker visibility because very little of the r_2 can be received by the

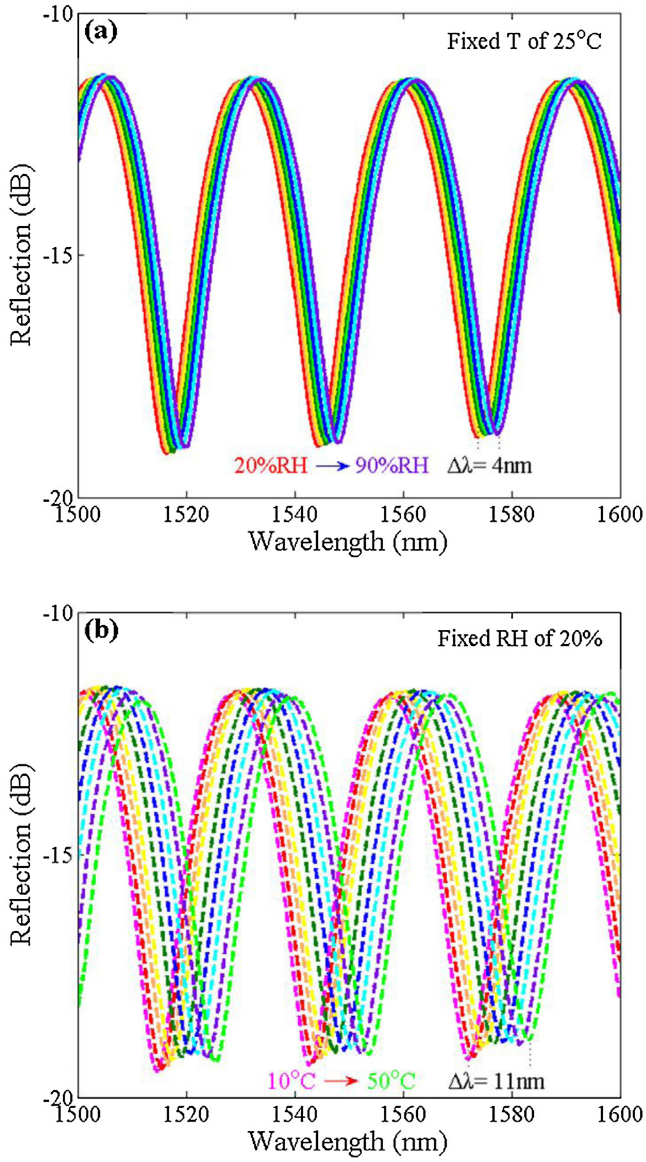

Fig. 5. Interference spectra of $L = 27\ \mu m$ PMFFI in response to only (a) *RH* and (b) *T* variations.

fiber core. If the amount of r_2 that is re-coupled into the core is much greater or much smaller than that of r_1, the visibility is low. On the other hand, structures of the sensors (2) and (3) make the r_2 approaching to their r_1 that would obtain better visibility.

4. Experimental results and discussion

Owing to the favorable hygroscopic capability of the NOA series of polymers, as revealed in our previous studies, the proposed PMFFI is employed to measure the surrounding *RH* to evaluate the effectiveness of the sensing scheme. The device is placed inside a temperature and humidity-controlled chamber (THCC), which was a closed space in which the *RH* was increased from 20% to 90% with *T* fixed at 25 °C, as displayed in Fig. 5(a). The used polymers with structures effectively adsorbed water molecules. In such the porous polymer systems response to the increase in humidity are caused by two processes: (1) the increase of the volume due to polymer swelling and (2) lowering of the refractive index due to the increased number of water molecules in the polymer. Each of these processes affects the interference pattern. The proposed

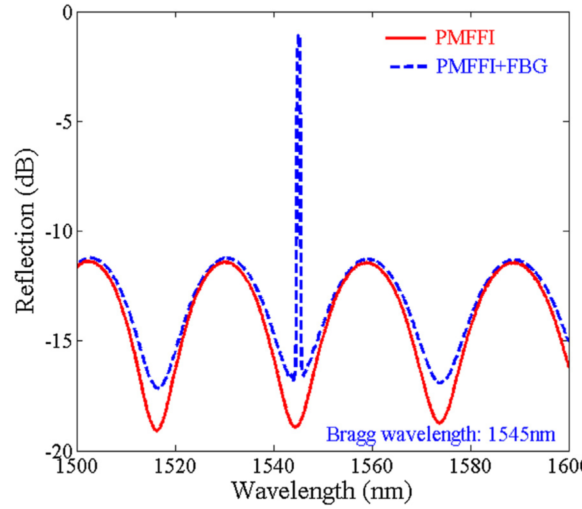

Fig. 6. Spectral responses of fabricated PMFFIs with (dashed line) and without (solid line) an FBG, respectively. Central wavelength of the FBG is 1545 nm.

PMFFI is also highly sensitive to variations in *T*. The highly sensitive dependence of the polymer on *T* arises mainly from the high TEC of the polymer, although the fact that some closed pores is filled with a few molecules of air and water vapor. The air and water vapor molecules inside the polymer are many fewer than the polymer molecules. To demonstrate this phenomenon, experiments are performed, yielding the results in Fig. 5(b), which indicates high sensitivity to *T* from $T = 10\,°C$ to 50 °C at a fixed *RH* of 20%. These results demonstrate that the spectral responses of such polymer-based fiber optic sensors are strongly correlated with *T* and *RH*. The measurement system may easily compensate for the *T* cross sensitivity by using an additional bare FBG that is not *RH* sensitive. Therefore, to measure simultaneously *RH* and *T*, the PMFFI is integrated with a general FBG, as described above. Fig. 6 plots the spectral responses of the fabricated PMFFIs with $L = 27\ \mu m$ with and without an FBG. The central wavelength of the FBG is around 1545 nm. The FBG herein is important in judging the variation in *T* because it is insensitive to the *RH*. The combined PMFFI + FBG sensor was tested in response to variations in *RH* and *T* in the chamber over an *RH* range of 20% to 90% and a *T* range of 10 °C to 50 °C. The wavelength shifts of the interference fringes were recorded when the chamber reached equilibrium at every humidity and temperature. Fig. 7(a) shows changes of the reflection spectra for the combined sensing probe as *RH* was increased. Insets (1) and (2) in Fig. 7(a) reveal the peak wavelength shifts of the FBG and PMFFI, respectively. A significant phase-shift of the interference fringes of PMFFI toward longer wavelengths is observed. The red-shift of the interference fringes at fixed $T = 25\,°C$ indicates slight expansion of the NOA61 polymer that causes changes in the optical path. However, the center resonant peak of the FBG is almost fixed, reflecting its insensitivity to *RH*. The linear curve fitting yields sensitivity to *RH* of 0.0545 nm/%*RH* during both desorption and adsorption. The result verifies the reversibility of *RH* measurement by the proposed PMFFI, which is shown in Fig. 7(b). The fitted lines reveal a proportional relationship between the wavelength shifts ($\Delta\lambda$) and *RH*, indicating that PMFFI responds linearly over the studied *RH* range. In contrast, the wavelength peak of the FBG is nearly fixed so the corresponding sensitivity is zero.

The integrated sensor was also utilized to sense *T* to study its thermal behaviors. Fig. 8(a) plots the relationships between *T* and the spectral responses at wavelengths region from 1500 nm to 1600 nm. The results demonstrate that the PMFFI and the FBG are both sensitive to *T* when the *RH* is fixed at 20%. Insets (1) and (2) present the peak wavelength shifts of the FBG and

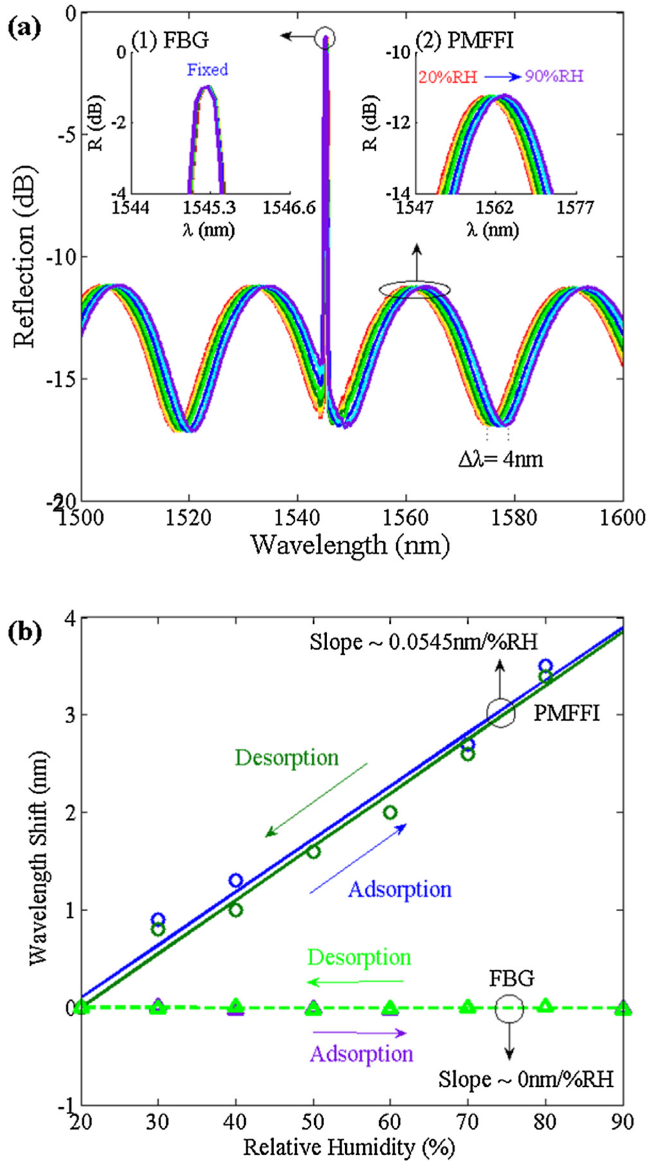

Fig. 7. (a) Reflection spectra of L = 27 μm PMFFI that incorporates FBG as RH increases. Insets (1) and (2) display shifts of peak wavelengths of FBG and PMFFI. (b) Sensitivities of proposed PMFFI and FBG to RH during adsorption and desorption processes.

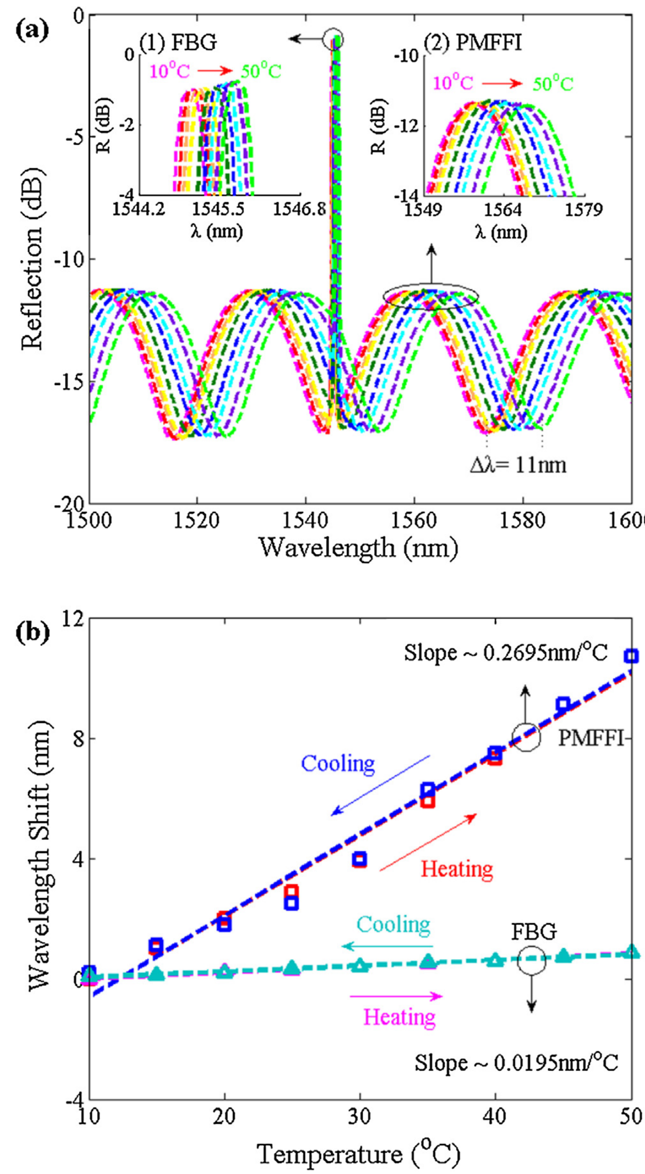

Fig. 8. (a) Reflection spectra of L = 27 μm PMFFI that incorporates FBG as T increases. Insets (1) and (2) present shifts of peak wavelengths of FBG and PMFFI. (b) Sensitivities of proposed PMFFI and FBG to T in heating and cooling.

PMFFI, respectively. The optical spectral shifts of the FBG and the PMFFI owing to the thermal expansion of the silica and NOA 61 are 0.78 nm and 10.8 nm, respectively over the T range of 20 °C~50 °C. The PMFFI is highly sensitive to T because of NOA 61 has a high thermal expansion coefficient. Fig. 8(b) plots the fitted linear wavelength shifts for the FBG and the PMFFI in response to variations in T. As T was increased and reduced, both PMFFI and FBG responded reversibly. The measured linear sensitivities of the PMFFI and FBG to T are determined to be 0.2695 and 0.0195 nm/°C, respectively. Based on the above experimental results, the aforementioned matrix inversion method is used to perform simultaneous measurement of RH and T. The sensitivities of the PMFFI and the FBG to RH are 0.0545 nm/%RH and 0 nm/%RH over an RH range 20–90%. The corresponding sensitivities to T are 0.2695 nm/°C and 0.0195 nm/°C, respectively, over the range of 20–50 °C. The normalized sensitivity parameters A', C' and B', D' are the T and RH sensitivity coefficients of the sensor, which are estimated to be 0.0195, 0.2695, 0 and 0.0545, respectively. Therefore, the following equations provide the basis for using the proposed PMFFI + FBG to measure simultaneously changes in T and RH once the $\Delta\lambda_{FBG}$ and $\Delta\lambda_{PMFFI}$ have been obtained.

$$\begin{pmatrix} \Delta T \\ \Delta RH \end{pmatrix} = \begin{pmatrix} 0.0195 & 0 \\ 0.2695 & 0.0545 \end{pmatrix}^{-1} \begin{pmatrix} \Delta\lambda_{FBG} \\ \Delta\lambda_{PMFFI} \end{pmatrix} \quad (8)$$

$$\begin{pmatrix} \Delta T \\ \Delta RH \end{pmatrix} = \frac{1}{1.06275 \times 10^{-3}} \begin{pmatrix} 0.0545 & 0.000 \\ -0.2695 & 0.0195 \end{pmatrix} \begin{pmatrix} \Delta\lambda_{FBG} \\ \Delta\lambda_{PMFFI} \end{pmatrix} \quad (9)$$

To demonstrate the accuracy of the Eq. (9) for the developed sensor, T and RH were simultaneously varied from their initial values of T_0 = 20 °C and ambient RH_0 = 50% to the three cases of (a) T = 30 °C, RH = 70%, (b) T = 10 °C, RH = 40%, and (c) T = 40 °C, RH = 35%. Table 1 presents the simultaneous measurement of T and RH under various conditions. Under the given condition of (a), the measured wavelength shifts of the FBG and the PMFFI are $\Delta\lambda_{FBG}$ = +0.188 nm and $\Delta\lambda_{PMFFI}$ = +3.75 nm, respectively. Based on the achieved Eq. (9), the variations of T and RH are readily obtained as ΔT = +9.64 °C and ΔRH = +21.15%, respectively. Thus, the measurement of the

Table 1
Simultaneous measurement of T and RH under various conditions.

Parameters	Conditions		
	(a) $T=30\,^\circ C$, $RH=70\%$	(b) $T=10\,^\circ C$, $RH=40\%$	(c) $T=40\,^\circ C$, $RH=35\%$
$\Delta\lambda_{FBG}$ (nm)	+0.188	−0.189	+0.379
$\Delta\lambda_{PMFFI}$ (nm)	+3.751	−3.085	+4.486
Determined data by Eq. (9)	$\Delta T=+9.64\,^\circ C$, $\Delta RH=+21.15\%$	$\Delta T=-9.69\,^\circ C$, $\Delta RH=-8.68\%$	$\Delta T=+19.44\,^\circ C$, $\Delta RH=-13.80\%$
Measured T_m and RH_m	$T_m=T_0+\Delta T=29.64\,^\circ C$, $RH_m=RH_0+\Delta RH=71.15\%$	$T_m=T_0+\Delta T=10.31\,^\circ C$, $RH_m=RH_0+\Delta RH=41.32\%$	$T_m=T_0+\Delta T=39.44\,^\circ C$, $RH_m=RH_0+\Delta RH=36.20\%$
$T_{error}=\lvert(T_m-T)/T\rvert$	$T_{error}=0.0120$	$T_{error}=0.0310$	$T_{error}=0.0140$
$RH_{error}=\lvert(RH_m-RH)/RH\rvert$	$RH_{error}=0.0164$	$RH_{error}=0.0330$	$RH_{error}=0.0343$

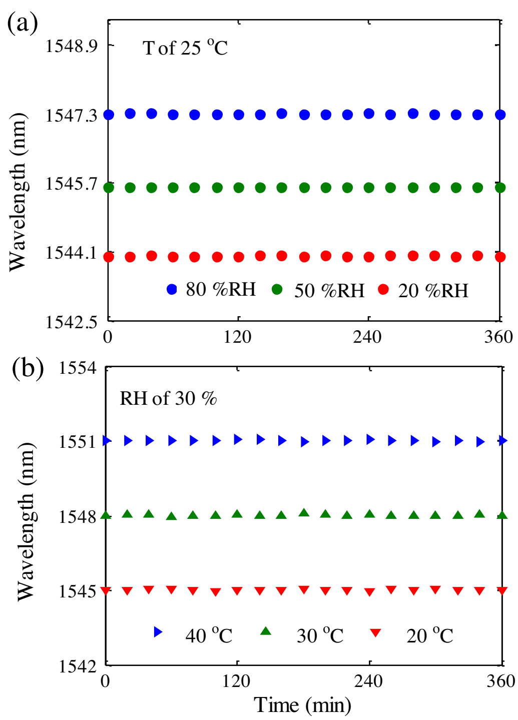

Fig. 9. Wavelength of spectral dip for various conditions of (a) RH and (b) T values based on long-term measurement.

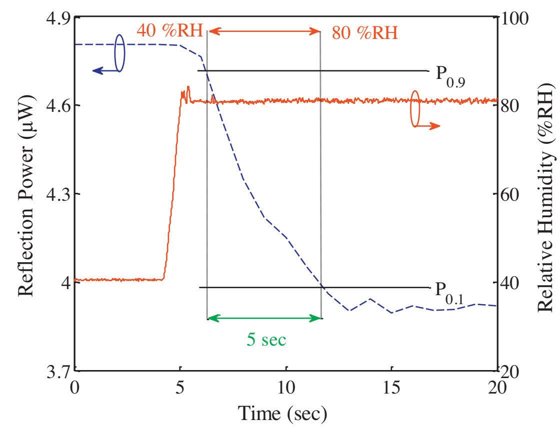

Fig. 10. Response transient of the sensor (dashed line) to increases in RH from 40% to 80% (soild line) at a fixed T of 25 °C.

T and RH in case (a) are measured as $T_m=20+9.64=29.64\,^\circ C$ and $RH_m=50+21.15=71.15\%$, respectively. The simultaneously measured values of T_m and RH_m are close to the actual values under condition (a), with only slight errors. The errors in T and RH are 1.2% and 1.6%, respectively. One can see other cases in Table 1, cases (b) and (c), the good performances of simultaneous sensing of the sensor have been achieved, with measurement errors of below 3.5%. The above evaluation demonstrates the feasibility of the proposed sensor. To examine the efficiency of the device, the stability and response time of the proposed polymer-sensor were measured. The proposed PMFFI was packaged and placed in the RH and T controlling chamber with various conditions of fixed RH and T for long-term measurement. The chamber included a compressor and two circulation fans to ensure that RH and T were uniform throughout the space. Therefore, mechanical vibrations and circulating airflows from the surroundings were present. The experimental results indicate the fixed interference dips of optical response that at various situation of RH and T for 6 h. The maximal variations in the wavelength dip in the various surroundings are averagely ±0.02 nm to demonstrate the operational stability of sensor, as displayed in Fig. 9(a) and (b).

In order to investigate the response transient of the NOA to the RH, the sensor was placed in the chamber again and subjected to rapidly changing RH from 40% to 80%. The curve of the change for RH is shown in the solid line of Fig. 10. The response of the optical signal was acquired using an optical power meter (Hewlett Packard 8153A Light wave Multimeter) and was plotted in the dashed line. The steep slope of the response verifies the effectiveness of the sensor. The response transient of the sensor is defined as the interval between reflections of 0.9 and 0.1. In the experiment, T is fixed at 25 °C and a response time of 5 s to an RH variation of 40% is obtained. The favorable response time may be attributed to the very tiny layer of the porous polymer on the fiber endface, which allows fast diffusion by the moisture molecules.

5. Conclusion

An optical fiber sensor that consists of a PMFFI and an FBG for the simultaneous measurement of RH and T is proposed and experimentally demonstrated. The optical gel, polymer NOA61, was utilized as a sensing material in an optical fiber humidity/temperature sensor that was based on a low finesse Fizeau interferometer. Owing to the strong hygroscopic characteristic of the porous polymer, a variation in RH affects the amount of water molecules that are adsorptive by it, varying the optical length of the cavity. The consequent wavelength shifts in the reflected interference pattern are proportional to the variations in RH and T. Experimental results reveal that the proposed sensor instantaneously detects both the T and RH of the surroundings. Owing to the miniature size of sensor, the response time to an RH change of approximately 40% is around 5 s. The results reveal that this simultaneous measuring device has many potential applications.

Acknowledgements

The authors would like to thank the National Science Council and Ministry of Science and Technology, Taiwan, for financially supporting this research under Contract No. NSC102-2221-E-239-033-MY3 and MOST 103-2622-E-239-003-CC3.

References

[1] C. Bariain, I.R. Matias, F.J. Arregui, M. Lopez-Amo, Optical fiber humidity sensor based on a tapered fiber coated with agarose gel, Sens. Actuators B: Chem. 69 (2000) 127–131.

[2] F.J. Arregui, I.R. Matias, K.L. Cooper, R.O. Claus, Simultaneous measurement of humidity and temperature by combining a reflective intensity-based optical fiber sensor and a fiber Bragg grating, IEEE Sens. J. 2 (2002) 482–487.

[3] S. Muto, O. Suzuki, T. Amano, M. Morisawa, A plastic optical fibre sensor for real-time humidity monitoring, Meas. Sci. Technol. 14 (2003) 746–750.

[4] L. Xu, J.C. Fanguy, K. Soni, S. Tao, Optical fiber humidity sensor based on evanescent-wave scattering, Opt. Lett. 29 (2004) 1191–1193.

[5] T.L. Yeo, T. Sun, K.T.V. Grattan, D. Parry, R. Lade, B.D. Powell, Characterisation of a polymer-coated fibre Bragg grating sensor for relative humidity sensing, Sens. Actuators B: Chem. 110 (2005) 148–155.

[6] J.M. Corres, F.J. Arregui, I.R. Matias, Design of humidity sensors based on tapered optical fibers, J. Lightwave Technol. 24 (2006) 4329–4336.

[7] J. Estella, P.D. Vicente, J.C. Echeverria, J.J. Garrido, A fibre-optic humidity sensor based on a porous silica xerogel film as the sensing element, Sens. Actuators B: Chem. 149 (2010) 122–128.

[8] J. Mathew, Y. Semenova, G. Rajan, G. Farrell, Humidity sensor based on photonic crystal fibre interferometer, Electron. Lett. 46 (2010) 1341–1343.

[9] S. Akitaa, H. Sasakia, K. Watanabea, A. Seki, A humidity sensor based on a hetero-core optical fiber, Sens. Actuators B: Chem. 147 (2010) 385–391.

[10] C.R. Zamarreno, M. Hernaez, I.D. Villar, I.R. Matias, F.J. Arregui, Tunable humidity sensor based on ITO-coated optical fiber, Sens. Actuators B: Chem. 146 (2010) 414–417.

[11] D. Viegas, M. Hernaez, J. Goicoechea, J.L. Santos, F.M. Araujo, F. Arregui, I.R. Matias, Simultaneous measurement of humidity and temperature based on an SiO_2-nanospheres film deposited on a long-period grating in-line with a fiber Bragg grating, IEEE Sens. J. 11 (2011) 162–166.

[12] L.H. Chen, T. Li, C.C. Chan, R. Menon, P. Balamurali, M. Shaillender, B. Neu, X.M. Ang, P. Zu, W.C. Wong, K.C. Leong, Chitosan based fiber-optic Fabry–Perot humidity sensor, Sens. Actuators B: Chem. 169 (2012) 167–172.

[13] J. Mathew, Y. Semenova, G. Farrell, Relative humidity sensor based on an agarose-infiltrated photonic crystal fiber interferometer, IEEE J. Sel. Top. Quantum Electron. 18 (2012) 1553–1559.

[14] T. Li, X. Dong, C.C. Chan, C.L. Zhao, P. Zu, Humidity sensor based on a multimode-fiber taper coated with polyvinyl alcohol interacting with a fiber Bragg grating, IEEE Sens. J. 12 (2012) 2205–2208.

[15] Z.F. Zhang, X.M. Tao, Synergetic effects of humidity and temperature on PMMA based fiber Bragg gratings, J. Lightwave Technol. 30 (2012) 841–845.

[16] W.C. Wong, C.C. Chan, L.H. Chen, T. Li, K.X. Lee, K.C. Leong, Polyvinyl alcohol coated photonic crystal optical fiber sensor for humidity measurement, Sens. Actuators B: Chem. 174 (2012) 563–569.

[17] L. Xia, L. Li, W. Li, T. Kou, D. Liu, Novel optical fiber humidity sensor based on a no-core fiber structure, Sens. Actuators A: Phys. 190 (2013) 1–5.

[18] T. Li, X. Dong, C.C. Chan, K. Ni, S. Zhang, P.P. Shum, Humidity sensor with a PVA-coated photonic crystal fiber interferometer, IEEE Sens. J. 13 (2013) 2214–2216.

[19] S. Zhang, X. Dong, T. Li, C.C. Chan, P.P. Shum, Simultaneous measurement of relative humidity and temperature with PCF-MZI cascaded by fiber Bragg grating, Opt. Commun. 303 (2013) 42–45.

[20] Y. Miao, K. Zhang, Y. Yuam, B. Liu, H. Zhang, Y. Liu, J. Yao, Agarose gel-coated LPG based on two sensing mechanisms for relative humidity measurement, Appl. Opt. 52 (2013) 90–95.

[21] L. Alwis, T. Sun, K.T.V. Grattan, Fibre optic long period grating-based humidity sensor probe using a Michelson interferometric arrangement, Sens. Actuators B: Chem. 178 (2013) 694–699.

[22] J. Mathew, Y. Semenova, G. Farrell, Experimental demonstration of a high-sensitivity humidity sensor based on an agarose-coated transmission-type photonic crystal fiber interferometer, Appl. Opt. 52 (2013) 3884–3890.

[23] X. Wang, C.L. Zhao, J. Li, Y. Jin, M. Ye, S. Jin, Multiplexing of PVA-coated multimode-fiber taper humidity sensors, Opt. Commun. 308 (2013) 11–14.

[24] J. Mathew, Y. Semenova, G. Farrell, Fiber optic hybrid device for simultaneous measurement of humidity and temperature, IEEE Sens. J. 13 (2013) 1632–1636.

[25] M. Shao, X. Qiao, H. Fu, N. Zhao, Q. Liu, H. Gao, An in-fiber Mach-Zehnder interferometer based on arc-induced tapers for high sensitivity humidity sensing, IEEE Sens. J. 13 (2013) 2026–2031.

[26] L. Alwis, T. Sun, K.V. Grattan, Analysis of polyimide-coated optical fiber long-period grating-based relative humidity sensor, IEEE Sens. J. 13 (2013) 767–771.

[27] J. Mathew, Y. Semenova, G. Farrell, Effect of coating thickness on the sensitivity of a humidity sensor based on an agarose coated photonic crystal fiber interferometer, Opt. Exp. 21 (2013) 6313–6320.

[28] J.S.I.M.R. Santosa Jr., C.M.B. Cordeirob, C.R. Biazolib, C.A.J. Gouveiac, P.A.S. Jorge, Characterisation of a Nafion film by optical fibre Fabry–Perot interferometry for humidity sensing, Sens. Actuators B: Chem. 196 (2014) 99–105.

[29] J. An, Y. Jin, M. Sun, X. Dong, Relative humidity sensor based on SMS fiber structure with two waist-enlarged tapers, IEEE Sens. J. 14 (2014) 2683–2686.

[30] H. Liu, H. Liang, M. Sun, K. Ni, Y. Jin, Simultaneous measurement of humidity and temperature based on a long-period fiber grating inscribed in fiber loop mirror, IEEE Sens. J. 14 (2014) 893–896.

[31] C.C. Liu, Y.W. You, L.G. Sheu, J.M. Hsu, C.L. Lee, Phenomenon of hygroscopicity in a fiber Fabry–Pérot interferometer with an absorbent polymer cavity, CLEO-PR & OECC/PS, 2013, pp. 1–2.

[32] J.H. Dai, Y.W. You, C.L. Lee, Probe typed polymer microcavity fiber Fizeau interferometer for humidity sensor, OECC/ACOFT (2014) 920–921.

[33] C.L. Lee, L.H. Lee, H.E. Hwang, J.M. Hsu, Highly sensitive air-gap fiber Fabry–Perot interferometers based on polymer-filled hollow core fibers, IEEE Photonics Technol. Lett. 24 (2012) 149–151.

[34] S. Park, J.W. Hong, Effect of liquid crystal structures on photopolymerization-induced phase separation behavior as determined from simultaneous resistivity and turbidity measurements, Polym. Test. 27 (2008) 428–433.

[35] L. Zheng, J. Vaillancourt, C. Armiento, X. Lu, Thermo-optically tunable fiber ring laser without any mechanical moving parts, Opt. Eng. 45 (7) (2006), 070503(2pp).

[36] https://www.norlandprod.com/adhesives/NOA%2061.html

Biographies

Cheng-Ling Lee received the Ph.D. degree from the Institute of Electro-Optical Engineering, National Chiao Tung University, Hsinchu, Taiwan, in 2003. During 2004–2010, she was an associate professor with the Department of Electro-Optical Engineering, National United University, Miaoli, Taiwan. In 2011, she became a full professor. Dr. Lee is the IEEE and OSA members and is the author of more than 40 peer reviewed publications in scientific journals. Her special fields of interests include fiber-based devices, optical fiber sensors and fiber gratings synthesis.

Yan-Wun You was born in 1990. He received the B.S. degree from National United University, Taiwan, in 2013. He is currently a master student with Department of Electro-Optical Engineering, National United University, Miaoli, Taiwan. His research interests include fiber based devices and optical fiber sensors.

Jia-Heng Dai was born in 1993. He is currently a senior student with Department of Electro-Optical Engineering, National United University, Miaoli, Taiwan. His research interests include fiber based devices and optical fiber sensors.

Jui-Ming Hsu received the B.S. degree in Department of Electronic Engineering from Chung-Yuan University, Chung-Li, Taiwan, in 1978, and the M.S. and Ph.D. degrees in optical sciences from the Institute of Optical Science, National Central University, Chung-Li, Taiwan, in 1994 and 1998. He had worked in the Chung Shan Institute of Science and Technology from 1980, and since 2006, he has been with the Department of Electro-Optical Engineering, National United University, Maioli, Taiwan, as an Assistant Professor and was promoted to an Associate Professor in 2013. His current research interests include fiber sensors, photonic crystal devices and fibers.

Jing-Shyang Horng received the Ph.D. degree from the Institute of Electronics, National Chiao Tung University, Taiwan, in 1988. He is now an associate professor with the Department of Electro-Optical Engineering, National United University, Taiwan. His special fields of interest include classical diffraction optics, packaging of laser modules, and characteristics testing of fiber optic transceiver modules. From July 1988 to July 1996, he was an engineer with Electro-Optical System Laboratory, Institute of Industrial Technology Research, Hsinchu, Taiwan.